Relaxing Jahn-Teller distortion of $LiMn_{0.6}Fe_{0.4}PO_4$ cathodes by Mg/Ni dual-doping for high-rate and long-life Li-ion batteries

Haifeng Yu[1,2#], Erdong Zhang[3#], Jinxun Yu[2], Songmin Yu[2], Yaoguo Fang[3], Ling Chen[1,2*], Hao Jiang[1,2*], Chunzhong Li[1,2]

[1] *Shanghai Engineering Research Center of Hierarchical Nanomaterials, School of Chemical Engineering, East China University of Science and Technology, Shanghai 200237, China*

[2] *Key Laboratory for Ultrafine Materials of Ministry of Education, School of Materials Science and Engineering, East China University of Science and Technology, Shanghai 200237, China*

[3] *Shanghai Xuanyi New Energy Development Co., Ltd, Shanghai 201800, China*

[*] Corresponding authors.

E-mail: chenling@ecust.edu.cn (Dr. L. Chen) and jianghao@ecust.edu.cn (Prof. H. Jiang)

Tel.: +86-21-64250949; Fax: +86-21-64250624.

1. Supporting Notes

Material characterization

The crystal structure of the samples was characterized using X-ray diffractometer (XRD, Bruker D8 Advance, Cu-Kα radiation) with a scan rate of 2 ° min^{-1}, and the lattice parameters were analyzed via GSAS Rietveld refinement software. The elemental content of the samples was detected by inductively coupled plasma optical emission spectrometer (ICP-OES, Agilent 725). The morphology, microstructure and element distribution were confirmed using scanning electron microscopy (SEM, Hitachi S-4800) and transmission electron microscopy (TEM, FEI Talos F200X) with energy dispersive spectrometry (EDS). Surface elemental valence states were analyzed by X-ray photoelectron spectroscopy (XPS, ESCALAB 250Xi, Al-Kα). A four-point probe semiconductor powder resistivity tester (RTS-1389, 4Probes Tech. Ltd., China) was used to tested the electrical conductivity of samples. The distribution of secondary particle size was measured by laser particle sizer (Microtrac S3500SI), and the primary particle size was summarized by Nano Measurer software. The differential scanning calorimeter (DSC) curves were obtained by a NETZSCH DSC204 machine. The cycled cells were disassembled, and the Li anode was dissolved in 0.1 M HNO_3. Then, this solution was carried out ICP-OES test to obtain the mass of dissolved Mn and Fe.

Electrochemical measurements

The cathodes, conductive agent (Super P, Cabot Corporation) and polyvinylidene fluoride (PVDF, Aladdin) were thoroughly mixed in N-methyl-pyrrolidone (NMP, Sigma-Aldrich) solvent at a mass ratio of 8 : 1: 1 to obtain the cathode slurries. The slurry was uniformly coated on an aluminum foil (active material loading of 2~3 mg cm^{-2}) and then dried at 120 °C for 12 h in a vacuum-drying oven. The as-obtained cathode electrode, polypropylene separator (Celgard 2400) and lithium metal anode (China Energy Lithium Co., Ltd.) were stacked in turn to prepare coin-type half cells in an argon-filled glove box, while the electrolyte (MJS energy

technology) was consisted of 1 M $LiPF_6$ in a mixture of ethylene carbonate/ethyl methyl carbonate/ dimethyl carbonate (V_{EC} : V_{EMC} : V_{DMC} = 1 : 1 :1). For a pouch-type full cells, the mass ratio of cathodes, Super P and PVDF was changed to 90 : 5: 5, and the loading mass was increased to 10~13 mg cm^{-2} with a compaction density of ~ 2.3 g cm^{-3}. The commercial graphite (Shanshan Technology) was used as anode materials with a N/P ratio in the range of 1.05~1.10. The galvanostatic current charge/discharge curves were tested on a LANDCT2003A battery tester at 25 °C with a voltage window of 2.5 V to 4.3 V (1C = 150 mAh g^{-1}). Cyclic voltammetry curves (CV) and electrochemical impedance spectra (EIS) were performed on an Autolab PGSTAT302N workstation.

2 Supporting Figures

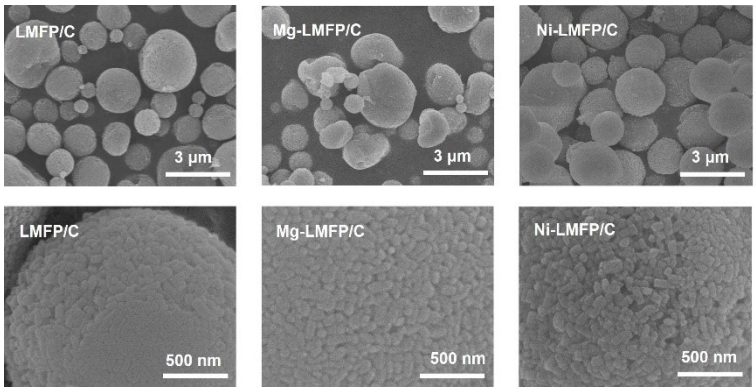

Fig. S1 The SEM images of LMFP/C, Mg-LMFP/C and Ni-LMFP/C.

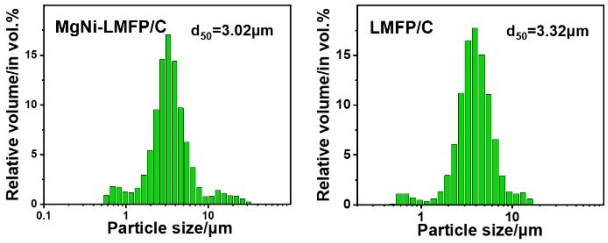

Fig. S2 The secondary particle size of MgNi-LFMP/C and LMFP/C.

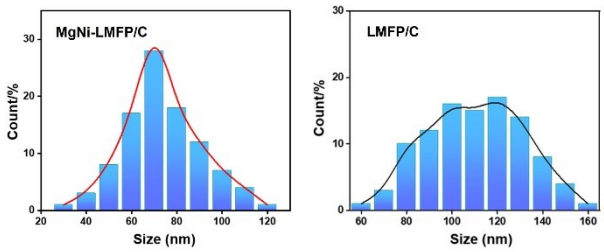

Fig. S3 The size distribution of primary particles for MgNi-LFMP/C and LMFP/C.

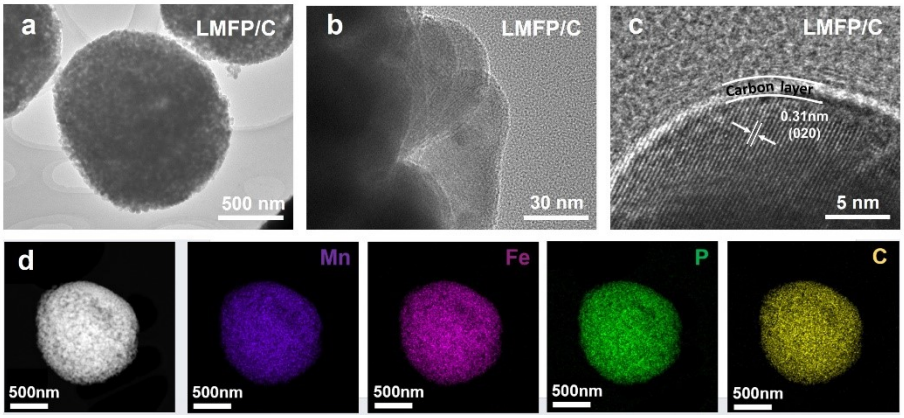

Fig. S4 TEM image and corresponding EDS mapping of LMFP/C.

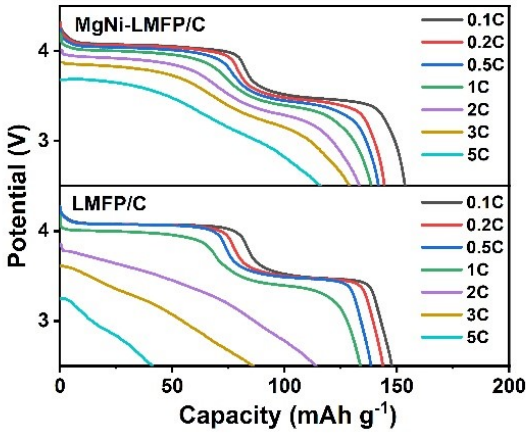

Fig. S5 The discharge curves at different current densities of MgNi-LMFP/C and LMFP/C.

Notes: At high current rates, the inhomogeneous Li-ion concentration distribution cannot ensure clear boundary between two phases, and thus the cathode will partially display solid-solution characterization. This will cause the voltage to gradually change with the Li-ion concentration, resulting in a sloping line. Besides, the increased polarization at high current cause the voltage to deviate from the thermodynamic equilibrium voltage, further contributing to the disappearance of the plateau and the appearance of a sloping

profile.

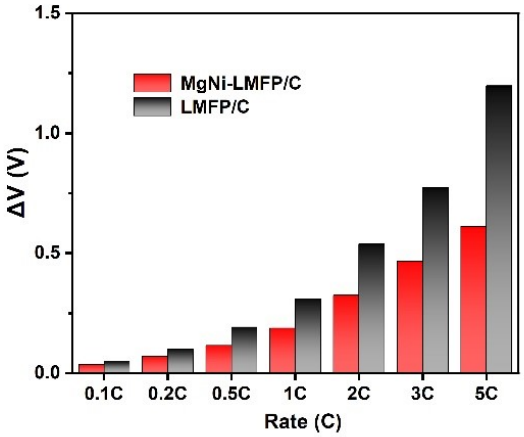

Fig. S6 The voltage hysteresis at different current densities of MgNi-LMFP/C and LMFP/C. The values were calculated according to average voltage differences between charging and discharging processes.

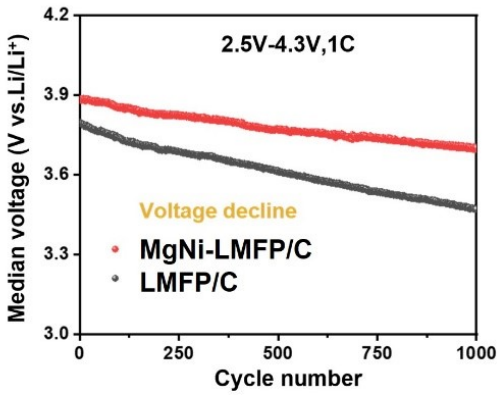

Fig. S7 The medium voltage during cycling at 1C of MgNi-LMFP/C and LMFP/C.

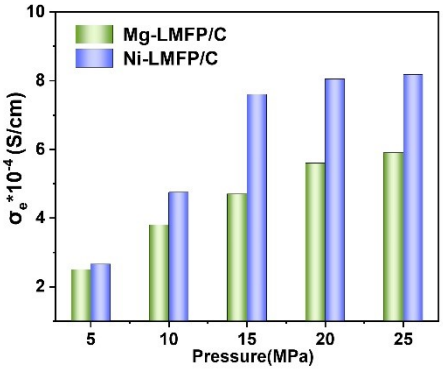

Fig. S8 Electronic conductivities at different pressures of Mg-LMFP/C and Ni-LMFP/C.

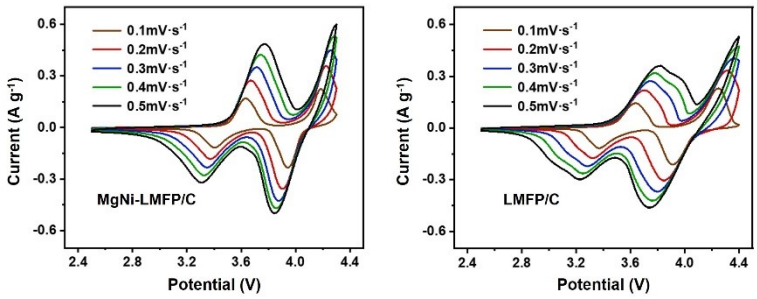

Fig. S9 The CV curves at various scan rates of MgNi-LMFP/C and LMFP/C.

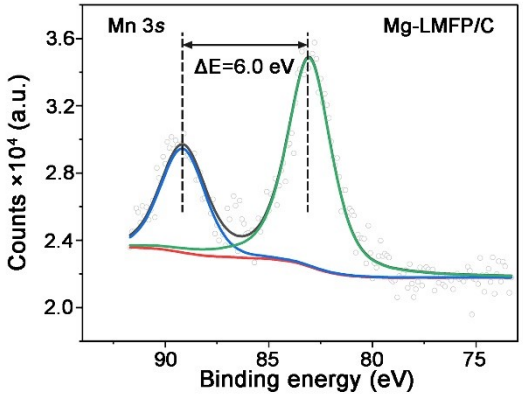

Fig. S10 Mn 3*s* XPS spectra of Mg-LMFP/C.

3 Supporting Tables

Table S1 The ICP-OES results of the LMFP-C, Mg-LMFP/C, Ni-LMFP/C and MgNi-LMFP/C.

Sample	Chemical composition（at%）			
	Mn	Fe	Mg	Ni
LMFP/C	59.9	40.1	/	/
LMFP/C-Mg	59.8	39.7	0.5	/
LMFP/C-Ni	59.6	39.9	/	0.5
LMFP/C-Mg,Ni	59.4	39.6	0.5	0.5

Table S2 XRD Rietveld refinement results of the LMFP-C, Mg-LMFP/C, Ni-LMFP/C and MgNi-LMFP/C.

Sample	Lattice parameters				Li-O bond length (Å)	R_{wp}(%)
	a(Å)	b(Å)	c(Å)	V(Å^3)		

LMFP/C	10.438	6.081	4.748	301.18	2.132	9.20%
LMFP/C-Mg	10.408	6.069	4.735	299.04	2.145	8.22%
LMFP/C-Ni	10.422	6.078	4.741	300.34	2.140	7.94%
LMFP/C-Mg,Ni	10.401	6.067	4.733	298.84	2.150	5.47%

Table S3 Electrochemical performance and cycle stability of LMFP cathodes reported in the literatures.

Samples	Voltage (V)	Capacity at 0.1C (mAh g^{-1})	Rate capability (mAh g^{-1})	Cycle performance	Reference
Mg,Ni-LMFP/C	2.5-4.3	152.0	115.0 (5C)	92.0% after 2000 cycles (full-cell)	This work
$LiMn_{0.7}Fe_{0.3}PO_4$	2.5-4.4	142.3	85.6 (2C)	73.3% after 500 cycles (full-cell)	1
$Li(Fe_{0.4}Mn_{0.6})_{0.97}Mg_{0.03}PO_4/C$	2.0-4.5 (CCCV)	153.6	138.8 (5C)	98.0% after 200 cycles (half-cell)	2
$Li(Fe_{0.6}Mn_{0.4})_{0.97}Ti_{0.03}PO_4/C$	2.5-4.5	163.5	94.1 (5C)	93.6% after 500 cycles (half-cell)	3
$Li_{0.97}Mg_{0.015}Mn_{0.8}Fe_{0.2}PO_4$	2.0-4.5	156.9	132.3 (5C)	93.5% after 500 cycles (half-cell)	4
Li_3VO_4-coated $LiMn_{0.5}Fe_{0.5}PO_4$	2.0-4.5	~152	125 (10C)	91.5% after 1000 cycles (half-cell)	5
$LiMn_{0.8}Fe_{0.2}PO_4$	2.5-4.25 (CCCV)	150	118 (5C)	~95% after 100 cycles (full-cell)	6
CNT-embedded $LiMn_{0.8}Fe_{0.2}PO_4/C$	2.3-4.5 (CCCV)	159.9	144.4 (5C)	72.9% after 100 cycles (full-cell)	7
$LiMn_{0.8}Fe_{0.15}Ni_{0.05}PO_4@C$	2.5-4.5	144.8	117.9 (5C)	88.7% after 500 cycles (half-cell)	8

Reference

[1] J. Liu, Y. Wu, B. Zhang, X. Xiao, Q. Hu, Q. Han, L. Wang, F. Bei and X. He, *Small*, 2024, **10**, 2309629.

[2] W. Lyu, W. Cai, T. Wang, X. Sun, E. Xu, J. Chen, K. Wu, Y. Zhang, *J. Energy Chem.*, 2024, **91**, 619-

627.

[3] J. Peng, Z. Li, Y. You, J. Liu, L. Wang, J. Xu, S. Ou, M. Yuan, *Ind. Eng. Chem. Res.*, 2024, **63**, 8228-8238.

[4] H. Hu, H. Li, Y. Lei, J. Liu, X. Liu, R. Wang, J. Peng, X. Wang, *J. Energy Storage*, 2023, **73**, 109006.

[5] M. Yu, J. Li and X. Ning, *Electrochim. Acta*, 2021, **368**, 137597.

[6] V. Borgel, G. Gershinsky, T. Hu, M. Theivanayagam and D. Aurbach, *J. Electrochem. Soc.*, 2013, **160**, A650-A657.

[7] J. Li, Y. Wang, J. Wu, H. Zhao and H. Liu, *J. Alloy Compd.*, 2018, **731**, 864-872.

[8] T. Zeng, P. Gao, Z. Zhou, C. Fan, Z. Liu, F. Zhang, J. Liu and J. Liu, *Energy Storage Mater.*, 2024, **65**, 103125